Supporting Information

Tailored Coupling of Biomineralized CdS Quantum Dots to rGO to Realize Ambient Aqueous Synthesis of a High-Performance Hydrogen Evolution Photocatalyst

John Sakizadeh[1], Joseph P. Cline[2], Mark A. Snyder[1], Christopher J. Kiely[1,2], Steven McIntosh[1]*

[1] Department of Chemical and Biomolecular Engineering. Lehigh University, Bethlehem, PA 18015, USA

[2] Department of Materials Science and Engineering, Lehigh University, Bethlehem, PA 18015, USA

*Corresponding author: mcintosh@lehigh.edu

Figure S1. *UV-vis absorption spectra of CdS/cys and rGO mixture at pH 4 before and after centrifugation demonstrating that there is no loss of CdS/cys signal that would be consistent with formation of a rGO-supported composite.*

Figure S2. *Images of photocatalyst at different points in the synthesis process. The images include (a) CdS/cys after enzymatic synthesis, (b) CdS/CA pellet after the ligand exchange, (c) resuspended CdS/CA at pH = 4, (d) CdS/CA/rGO pellet after assembly, and (e) resuspended CdS/CA/rGO. Images (a), (c), (d) demonstrate the stability of the suspensions.*

Figure S3. *(A, B) A low magnification HAADF- and BF-STEM image pair of a graphene sheet loaded with CdS and Pt; (C, D) a higher magnification HAADF- and BF-STEM image pair of the graphene sheet showing a non-uniform distribution of CdS and Pt on the support E, F) a selected area diffraction pattern from an uncoated region of the support material, , and F) analysis of the measured interplanar spacings and angles from E showing a match to the [001] zone axis of graphene.*

Figure S4*. Inverse Fast Fourier Transform (IFFT) processed image of a zincblende type CdS particle oriented along the [310] direction.*

Table S1. *Measured lattice spacings and interplanar angles derived by FFT analysis of the CdS nanocrystal shown in Figure 2c compared with theoretical values for wurtzite-type CdS viewed along [111].*

Table S2. *Measured lattice spacings and interplanar angles derived by FFT analysis of the CdS nanocrystal shown in Figure S4 compared with theoretical values for zincblende-type CdS viewed along [310].*

Figure S5. *(a) UV-vis absorption spectra of washed and sonicated CdS/CA/rGO demonstrating control of the mass of CdS adsorbed to rGO by adding the same mass of rGO to different dilutions of as-synthesized CdS/CA sol. H_2 production rate optimization for CdS/CA/rGO with respect to (b) wt%, (c) and total mass of rGO added.*

Figure S6. *H_2 production rate optimization of CdS/CA/rGO with respect to cysteamine concentration used during ligand exchange.*

Figure S7. *Photoluminescence data of photocatalyst sample shows significant decrease in P.L. intensity after cys ligand exchange with CA and adsorption onto rGO.*

Figure S8. *a) Biexponential and b) triexponential fits to the time-correlated single photon counting (TCSPC) data and corresponding instrument response function (IRF).*

Table S3. *Lifetimes and amplitudes obtained from fitting a biexponential decay function to time-correlated single photon counting (TCSPC) data.*

Table S4. *Lifetimes and amplitudes derived from fitting a triexponential decay function to time-correlated single photon counting (TCSPC) data.*

Figure S9. *HAADF-STEM micrograph of Pt/CdS/rGO agglomerate spanning a hole in the supporting holey carbon film.*

Figure S10. *Inverse Fast Fourier Transform (IFFT) processed image of an individual Pt particle in the Pt/CdS/rGO sample oriented along the [110] direction.*

Table S5. *Measured lattice spacings and interplanar angles derived by FFT analysis of the lattice image of the Pt nanocrystal shown in Figure S10 compared with theoretical values for face centered cubic Pt viewed along [110].*

Figure S11. *Absorbance and photoluminescence UV-vis spectra of the as-synthesized CdS/cys nanocrystals.*

Figure S12. *UV-vis absorption spectrum of GO and rGO. The UV-vis spectrum of GO shows characteristic peaks at 230 nm and 300 nm attributed to aromatic carbons and carbonyl groups, respectively. The UV-vis spectrum of rGO has a single peak at 260 nm, indicating the growth of the aromatic regions on rGO compared to GO.*

Figure S13. *Photocatalytic hydrogen production of CdS/CA using 200 mM total of different sacrificial reagent. It was found that CdS was more active than sulfur-based sacrificial reagent in comparison to methanol.*

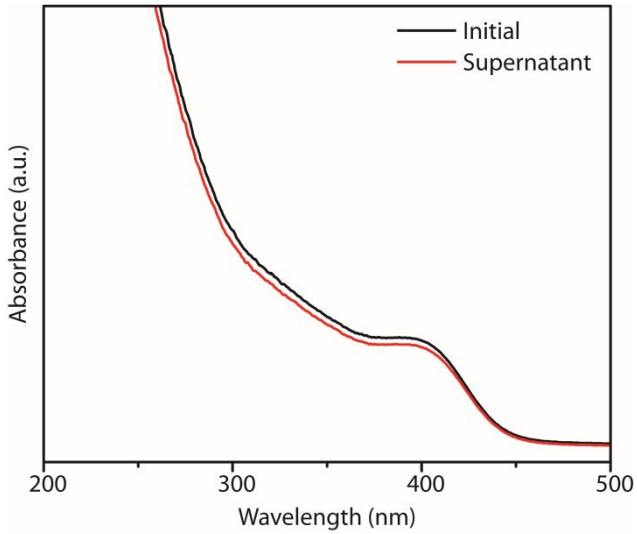

Figure S1. *UV-vis absorption of CdS/cys and rGO mixture at pH 4 before and after centrifugation demonstrating that there is no loss of CdS/cys signal that would be consistent with formation of a rGO-supported composite.*

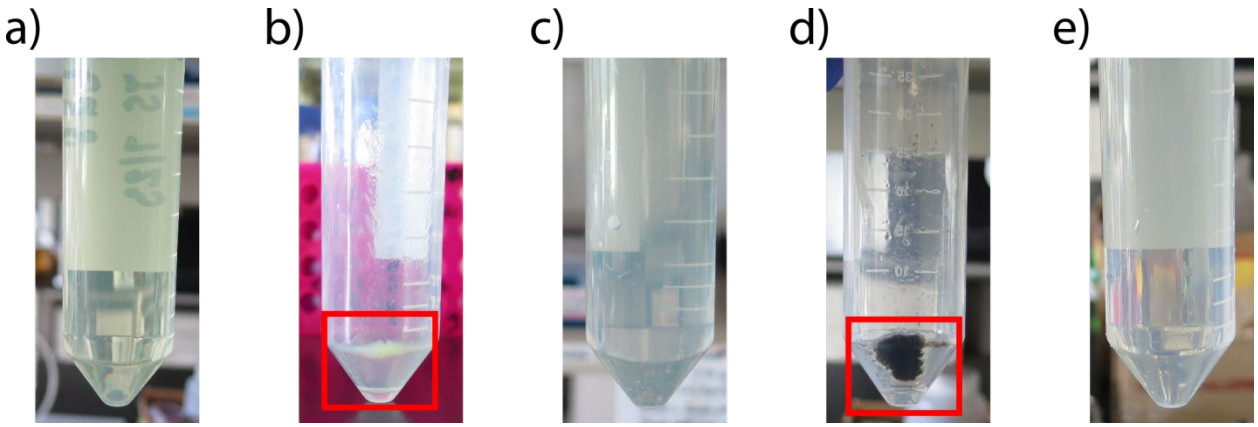

Figure S2. *Images of photocatalyst at different points in the synthesis process. The images include (a) CdS/cys after enzymatic synthesis, (b) CdS/CA pellet after the ligand exchange, (c) resuspended CdS/CA at pH = 4, (d) CdS/CA/rGO pellet after assembly, and (e) resuspended CdS/CA/rGO. Images (a), (c), (d) demonstrate the stability of the suspensions.*

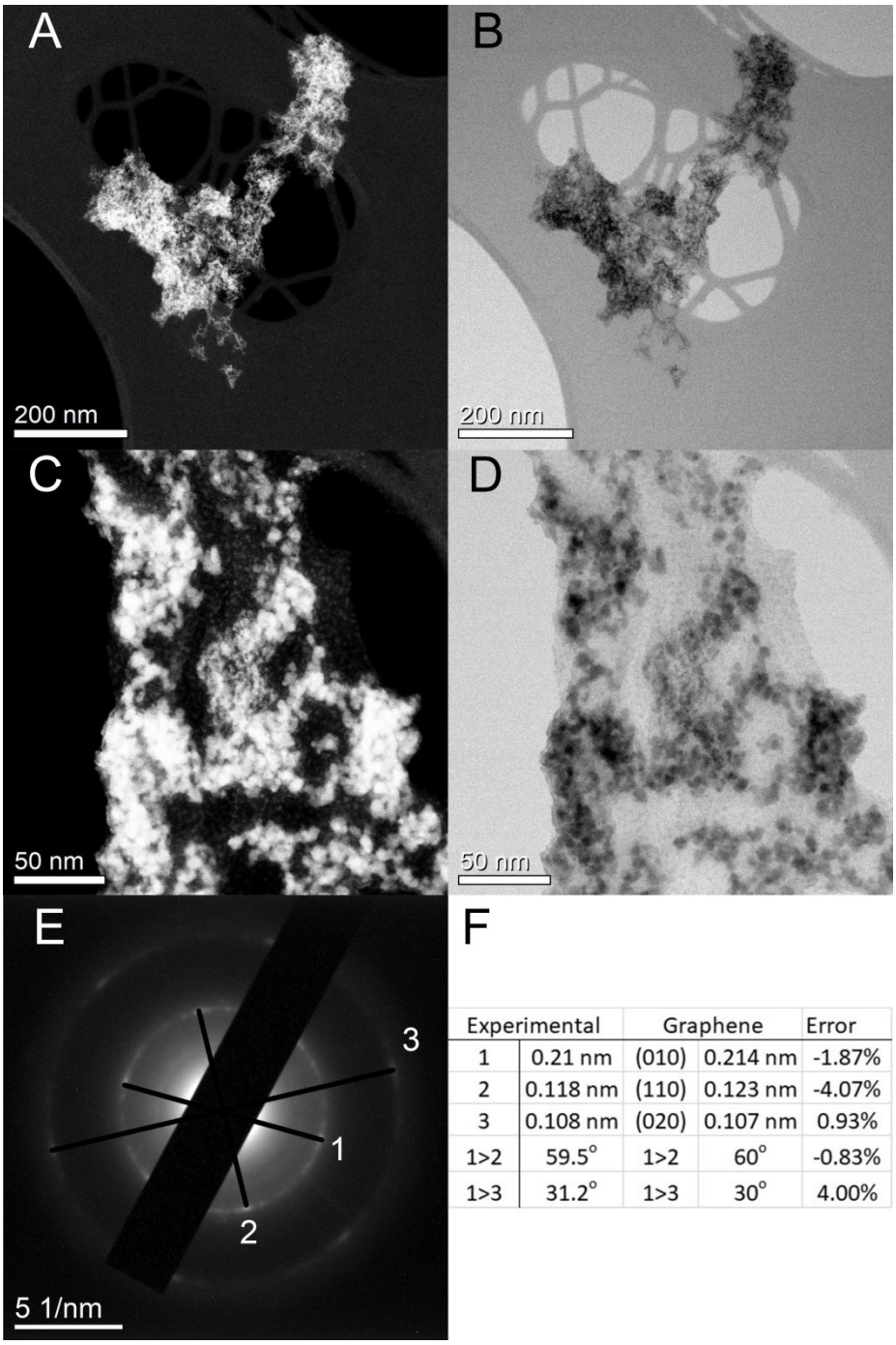

Experimental		Graphene		Error
1	0.21 nm	(010)	0.214 nm	-1.87%
2	0.118 nm	(110)	0.123 nm	-4.07%
3	0.108 nm	(020)	0.107 nm	0.93%
1>2	59.5°	1>2	60°	-0.83%
1>3	31.2°	1>3	30°	4.00%

Figure S3. *(A, B) A low magnification HAADF- and BF-STEM image pair of a graphene sheet loaded with CdS and Pt; (C, D) a higher magnification HAADF- and BF-STEM image pair of the graphene sheet showing a non-uniform distribution of CdS and Pt on the support E, F) a selected area diffraction pattern from an uncoated region of the support material, , and F) analysis of the measured interplanar spacings and angles from E showing a match to the [001] zone axis of graphene.*

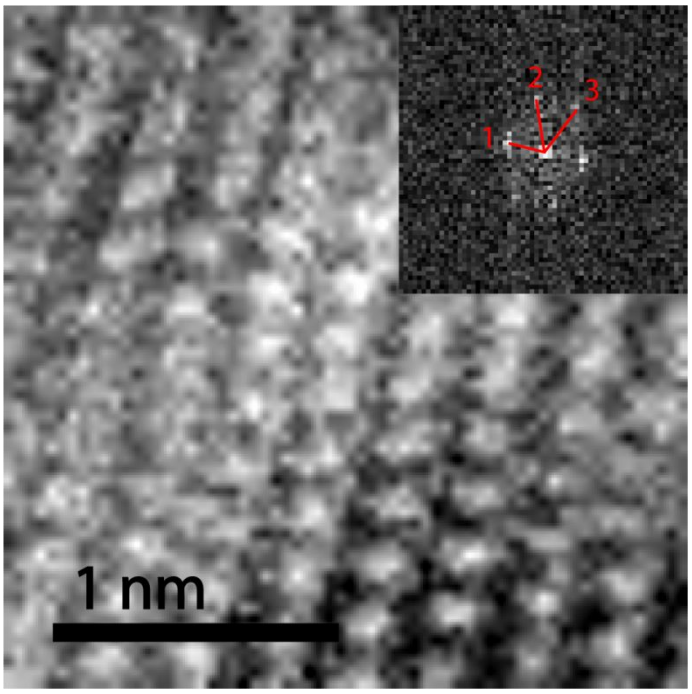

Figure S4. *Inverse Fast Fourier Transform (IFFT) processed image of a zincblende type CdS particle oriented along the [310] direction.*

Table S1. *Measured lattice spacings and interplanar angles derived by Fast Fourier Transform (FFT) analysis of the CdS nanocrystal shown in Figure 2c compared with theoretical l values for wurtzite-type CdS viewed along [111].*

Plane	(hkl)	Measured d (Å)	Expected d (Å)	Error (%)	2 Planes	Measured Angle (deg)	Expected Angle (deg)	Error (%)
1	(101)	3.18	3.22	-1.09	1-2	48.3	49.9	-3.05
2	$(1\bar{1}2)$	2.47	2.49	-0.96	1-3	41.1	40.1	2.27
3	(110)	2.10	2.10	-1.09	2-3	90.5	90	0.58

Table S2. *Measured lattice spacings and interplanar angles derived by fast fourier transform (FFT) analysis of the CdS nanocrystal shown in Fig S4 compared with theoretical values for zincblende-type CdS viewed along [310].*

Plane	(hkl)	Measured d (Å)	Expected d (Å)	Error (%)	2 Planes	Measured Angle (deg)	Expected Angle (deg)	Error (%)
1	(002)	2.83	2.97	-4.71	1-2	70.35	72.4	-2.83
2	$(1\bar{3}1)$	1.91	1.79	6.70	1-3	44.0	46.5	-5.38
3	$(1\bar{3}3)$	1.29	1.36	-5.15	2-3	27.2	25.9	5.02

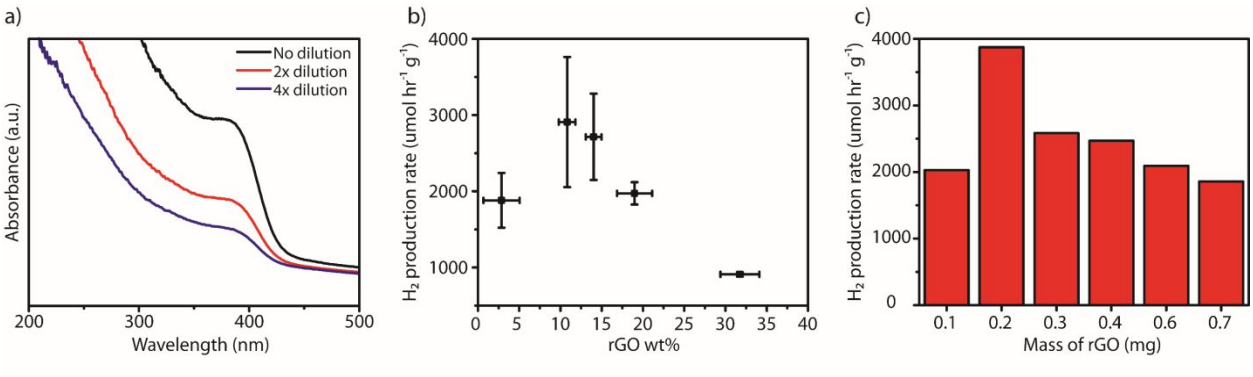

Figure S5. *(a) UV-vis spectra of washed and sonicated CdS/CA/rGO demonstrating control of the mass of CdS adsorbed onto rGO by adding the same mass of rGO to different dilutions of as-synthesized CdS/CA sol. H_2 production rate optimization for CdS/CA/rGO with respect to (b) wt%, (c) and total mass of rGO added.*

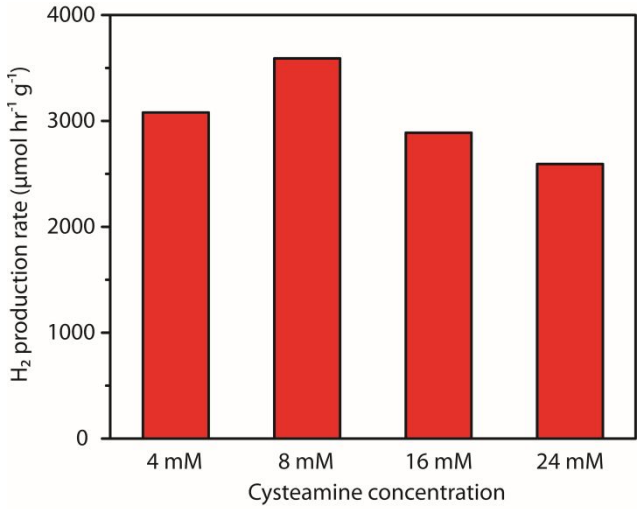

Figure S6. *H_2 production rate optimization of CdS/CA/rGO with respect to cysteamine concentration used during ligand exchange.*

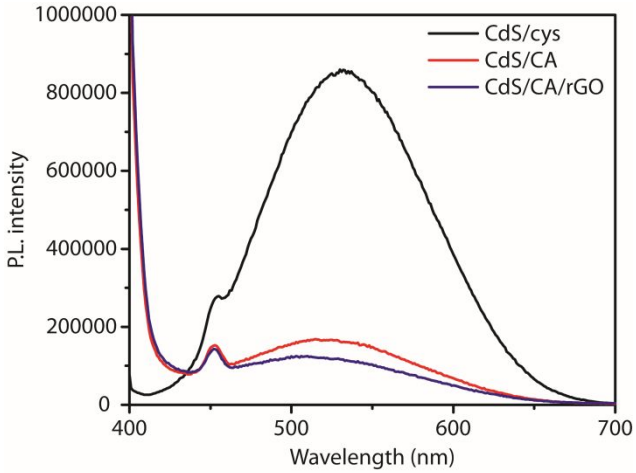

Figure S7. *Photoluminescence data of photocatalyst sample shows significant decrease in P.L. intensity after cys ligand exchange by CA and adsorption onto rGO.*

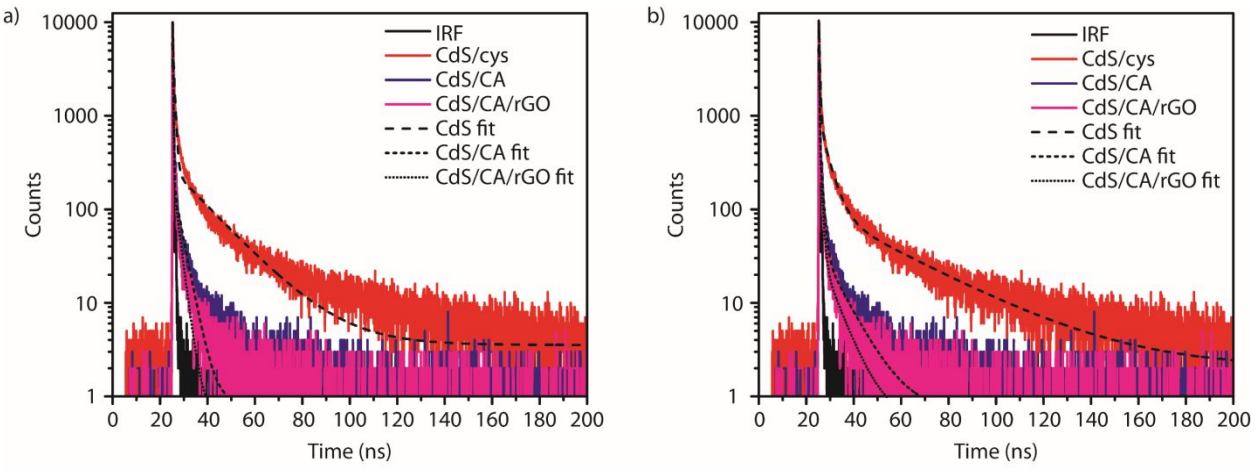

Figure S8. *a) Biexponential and b) triexponential fits to the time-correlated single photon counting (TCSPC) data and the corresponding instrument response function (IRF).*

Table S3. *Lifetimes and amplitudes obtained from fitting a biexponential decay function to time-correlated single photon counting (TCSPC) data.*

Sample	τ_1 (s)	τ_2 (s)	a_1	a_2	X^2 *
CdS/cys	6.3E-10	1.6E-08	2.4	8.1E-02	4.8
CdS/CA	1.9E-10	3.3E-09	5.0	6.1E-02	1.3
CdS/CA/rGO	1.7E-10	2.2E-09	5.4	6.7E-02	0.96

Table S4. *Lifetimes and amplitudes derived from fitting a triexponential decay function to time-correlated single photon counting (TCSPC) data.*

Sample	τ_1 (s)	τ_2 (s)	τ_3 (s)	a_1	a_2	a_3	X^2 *
CdS/cys	3.7E-09	3.2E-08	3.4E-10	0.26	3.0E-02	3.6	1.8
CdS/CA	1.0E-09	8.8E-09	1.6E-10	0.23	1.2E-02	5.7	0.77
CdS/CA/rGO	8.34E-10	6.5E-09	1.4E-10	0.21	1.0E-02	5.8	0.67

*The chi-squared (X^2) values of the fitted exponential decay functions, which are a measure of model fit, were calculated. The X^2 was defined as the sum of the mean squared errors divided by the standard deviation and degrees of freedom. A X^2 value close to unity indicates that the model fits the data well. Due to high X^2 values of the biexponential fits, the fluorescence lifetime data was also fitted to a triexponential function.

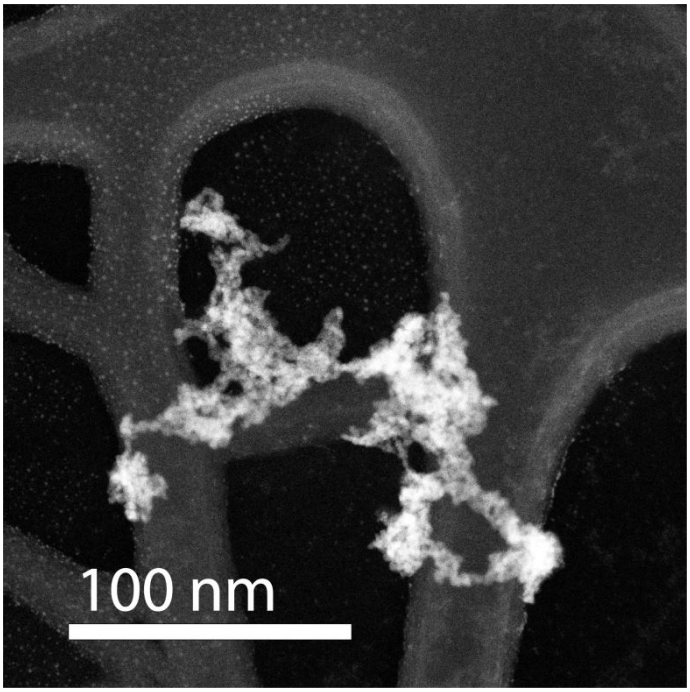

Figure S9. *TEM micrograph of a Pt/CdS/rGO agglomerate spanning a hole in the supporting holey carbon film.*

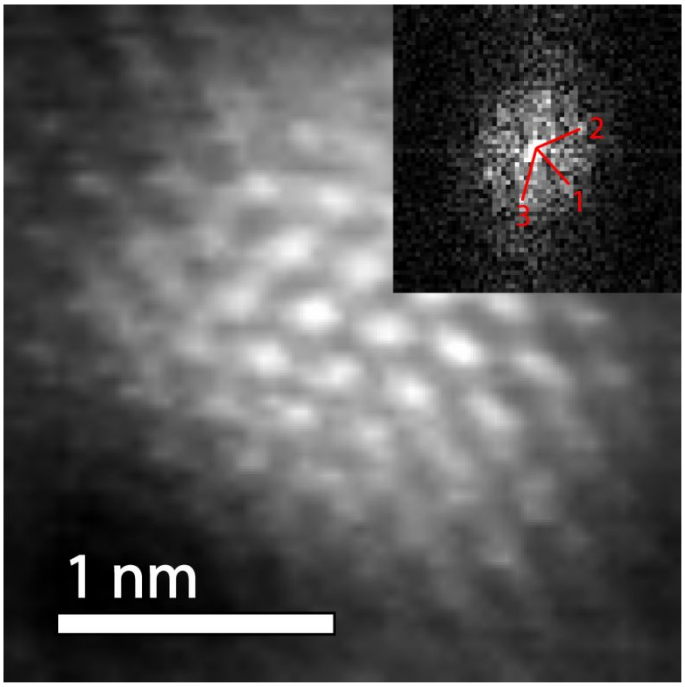

Figure S10. *Inverse Fast Fourier Transform (IFFT) processed image of an individual Pt particle in the Pt/CdS/rGO sample oriented along the [110] direction.*

Table S5. *Measured lattice spacings and interplanar angles derived from FFT analysis of the lattice image of of the individual Pt nanocrystal shown in Figure S10 compared with theoretical values for face centered cubic Pt viewed along [110].*

Plane	(hkl)	Measured d (Å)	Expected d (Å)	Error (%)	2 Planes	Measured Angle (deg)	Expected Angle (deg)	Error (%)
1	$(1\bar{1}\bar{1})$	2.24	2.26	-0.88	1-2	71.7	70.5	1.70
2	$(11\bar{1})$	2.25	2.26	-0.44	1-3	52.8	54.7	-3.47
3	(020)	1.98	1.96	1.02	2-3	128.5	125.3	2.55

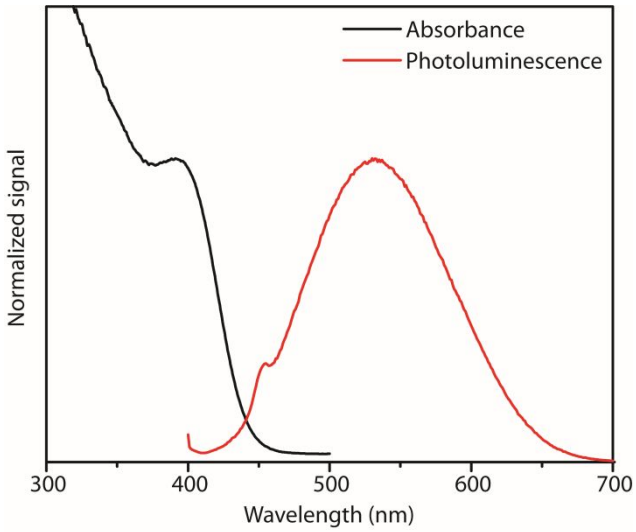

Figure S11. *Absorbance and photoluminescence UV-vis spectra of the as-synthesized CdS/cys nanocrystals.*

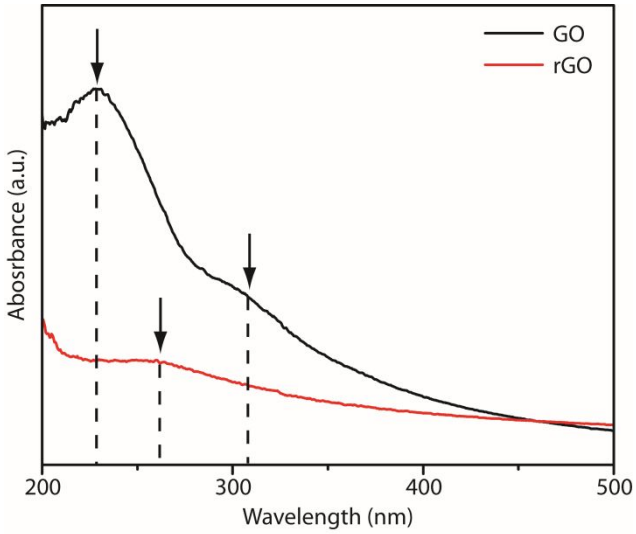

Figure S12. *UV-vis absorption spectrum of GO and rGO. The UV-vis spectrum of GO shows characteristic peaks at 230 nm and 300 nm attributed to aromatic carbons and carbonyl groups, respectively. The UV-vis spectrum of rGO has a single peak at 260 nm, indicating the growth of the aromatic regions on rGO compared to GO.*

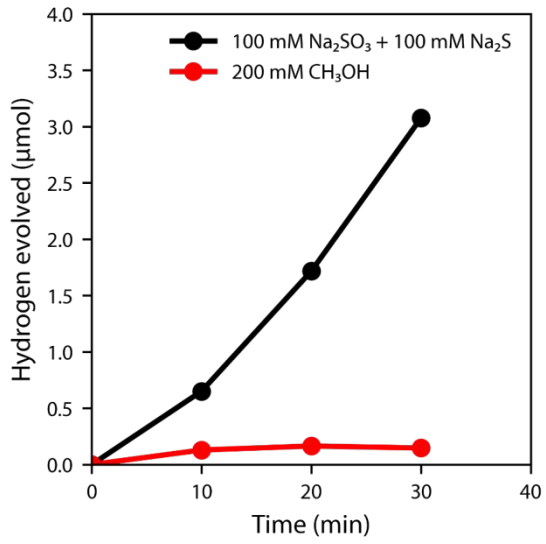

Figure S13. *Photocatalytic hydrogen production of CdS/CA using 200 mM total of different sacrificial reagent. It was found that CdS was more active than sulfur-based sacrificial reagent in comparison to methanol.*